Resistive switching behaviour of nickel nanoparticles embedded naphthalene sulfonic acid doped polyaniline nanocomposites

Madhumita Bhaumik[a*], Arjun Maity[b,c], Hendrik G. Brink[c], Zolile Wiseman Dlamini[a], SrinivasuVijaya Vallabhapurapu[a]

[a]*Department of Physics, University of South Africa, Florida Park,1709, South Africa*
[b]*DST/CSIR, Centre for Nanostructure and Advanced Materials (CeNAM), Council for Scientific and Industrial Research (CSIR), Pretoria 0001, South Africa*
[c]*Chemical Engineering Department, University of Pretoria, South Africa.*

---

*Corresponding author: E-mail addresses: bhaumikmadhu@gmail.com (M. Bhaumik).

Abstract

Hybrid nanocomposite materials comprising of organic polymer and inorganic metal nanoparticles with unique properties are popular for their advanced technological applications including resistive switching memory devices. Herein, nanocomposites (NCs) of 2-naphthalene sulfonic acid doped polyaniline nanotubes (PANI-NSA NTs) and nickel nanoparticles (Ni NPs) were synthesized via a facile chemical synthesis procedure where metallic Ni nanoparticles were embedded/deposited onto surface of PANI-NSA NTs by a simple reduction method. Different characterization methods revealed successful deposition of weak ferromagnetic Ni NPs onto the PANI-NSA matrix. The bipolar resistive switching behaviour of the as synthesized PANI-NSA+Ni NCs was explored under the application of voltage stress in a two terminal sandwiched device configuration. The fabricated Indium Tin Oxide/PANI-NSA+Ni/Silver (ITO/PANI-NSA+Ni/Ag) device displayed bipolar resistive switching property having a memory window of $\sim 1.5 \times 10^3$, and switches effectively over 200 cycles. Ohmic conduction at lower voltage regime and space charge limited Mott–Gurney current conduction model at higher voltage region were identified as major charge conduction mechanism in the HRS of the device. On the other hand, in the entire LRS region experimental data followed Mott-Gurney conduction model.

Keywords: Polyaniline, Nickel nanoparticles, Nanotubes, Ferromagnetic, Resistive switching

1. Introduction

Recently, tremendous advancement in data storage device technology have governed to the search for high-performance, cost-effective memory devices which could overcome the limitations of conventional silicon-based device technology. The device architecture comprising of two metal electrodes and a thin film of an active material sandwiched between the electrodes whenever showed electrical switching amongst high resistive state (HRS) to low resistive state (LRS) under the application of a voltage stress is considered as a device called resistive random-access memory (ReRAM) [1,2]. In data storage technique the HRS is equivalent to digital “0” state and LRS can be regarded as digital “1” state. Moreover, ReRAM possess superior potential to fulfil high density data storage capacity, quick access, rapid transfer of data, low power consumption as well as neuromorphic computing which could comply with the needs for data storage with ultrahigh density capacity and for artificial intelligent technologies [3-5]. Numerous materials including inorganic compounds, organic materials and inorganic-organic hybrids have been explored as active components of resistive switching devices [6-20].

Among others, organic and inorganic-organic hybrids/composites have stimulated attention of the scientific community owing to their unique properties like high performance, light weight, flexibility, high scalability, low cost and, most significantly, easy implication of solution-processing techniques such as inkjet printing and screen printing for large-area roll-to-roll fabrication of the thin film devices [21-23].

Within the class of organic polymeric materials, the intrinsically conducting nanostructured polyaniline (PANI) is very popular polymer. Unique properties such as tunable electrical conductivity, adjustable doping and de-doping effect, pH-sensitive, reversable redox reaction properties, light weight, and good environmental stability of PANI have made it an excellent choice for various applications [24-27]. These include gas sensors, supercapacitors, adsorbent, electrocatalysis etc. [28-33].

As PANI polymer and its nanocomposites having excellent tunable electrical properties, several studies have explored their resistive switching properties for ReRAM device applications [34-42]. However, it is still imperative to explore new material with higher resistive switching performance applicable to ReRAM devices. Meanwhile, inclusion of metallic nanoparticles into the PANI matrix can exhibit functional resistive switching property whereas PANI can perform as current limiting counterpart. In an effort to examine the resistive switching behaviour of nanostructure PANI based nanocomposites, we have synthesized magnetic nickel (Ni) nanoparticles embedded 2-nathalene sulfonic acid doped PANI (PANI-NSA) nanotubes. Various physico-chemical techniques were used for morphological and structural characterization of PANI-NSA+Ni NCs. Resistive switching property of the two terminal ITO/PANI-NSA+Ni/Ag device was studied under the application of a voltage stress. Detailed charge transport and resistive switching mechanism were also explored for the first time.

2. Materials and experimental methods

2.1. Materials

The monomer aniline (ANI,) with 99% purity achieved from Sigma Aldrich, USA, used for the PANI synthesis, was purified through the process of double distillation, then preserved at 0–5 °C temperature before use. The dopant 2-naphthalene sulfonic acid (2-NSA) with 70% purity, the oxidant ammonium persulfate (APS, 98% purity) utilized for polymerization, metal precursor Ni (II) chloride hexahydrate, hydrazine hydrate (HH, 50–60%) used as reductant, ethylene glycol (EG) and sodium hydroxide (NaOH), polyvinylpyrrolidone (PVP 360) polymer used for film formation of nanocomposites were also procured from the same chemical company.

2.2. PANI-NSA nanotubes synthesis

Nanotubes of 2-NSA doped PANI polymer, were synthesized as follow: 0.2 mL ANI monomer, and 0.208 g of 2-NSA, were added into 80 mL of de-ionized water while the mixture was stirred with a magnetic stirrer and the reaction temperature was kept constant between 0–3 °C for 30 minutes. Afterwards, to the ANI-2-NSA reaction mixture, an aqueous solution of APS (0.456 g in 5 mL de-ionized water) was added. Subsequently, the process of stirring was continued for additional 1 minute. The above reaction solution was conserved at 0–3 °C without stirring for 24 hours to complete of the polymerization reaction. After that, 2-NSA doped PANI (PANI-NSA) polymer was filtered through vacuum filtration and washed thoroughly with deionized water and methanol followed by drying for 24 hours at 60 °C in a vacuum oven.

2.3. PANI-NSA+Ni nanocomposites synthesis

The nanocomposites of nanotubular PANI-NSA coated with Ni nanoparticles were manufactured by depositing metallic Ni nanoparticles onto the previously synthesized PANI-NSA nanotubes surface/matrix by a reduction process. For the formation of Ni nanoparticles onto the surface of PANI-NSA nanotubes, 0.2 g powder of PANI-NSA polymer being dispersed onto the solution of ethylene glycol (20 mL) and $NiCl_2$, $6H_2O$ (0.404 g) through mechanical stirring. Afterwards, addition of 5 mL HH and 2 mL NaOH (1M) solution into the (PANI-NSA + Ni^{2+} + EG) dispersion leading to the reductive formation of Ni nanoparticles with metallic in nature on top of the PANI-NSA nanotubes surface. The whole reduction reaction was accomplished at 60 °C in an oil bath for 3 hours. The as obtained PANI-NSA+Ni nanocomposites with ~ 33.3 wt % Ni nanoparticles loading were filtered, washed by deionized water, subsequently with ethanol. Lastly, the nanocomposites were vacuum dried at 60 °C for 24 hours.

2.4. Characterization techniques

A Carl Zeiss, Germany Focussed Ion Beam-Scanning Electron Microscope (FIB-SEM) and a JEOL JEM-2100 (from, Japan) transmission electron microscope (TEM) with high resolution (HR) imaging system, were utilized to envisage the morphology and size of the PANI-NSA polymer and PANI-NSA+Ni NCs, respectively. Various chemical bonding of the PANI-NSA+Ni NCs were determined using the Fourier transformed infrared (FTIR) spectrum achieved through FTIR Spectrum 100 spectrometer with attenuated total reflection (ATR) facility obtained from Perkin–Elmer, USA. Crystalline structure of bare PANI-NSA and its PANI-NSA+Ni NCs counterparts was examined by using a X'Pert PRO diffractometer from PANalytical. Elemental composition analysis and detection of oxidation state of the formed Ni NPs were performed by X-ray photoelectron spectroscopic (XPS) measurements with Thermo-Scientific (USA) ESCALAB 250Xi XPS spectrometer where a monochromatic Al X-ray source was used. Magnetic property of the nanocomposites of PANI-NSA+Ni was explored by the Vibrating Sample Magnetometer (VSM) measurement option of a Physical Property Measurements system (PPMS Evercool-II), from Quantum Design, USA.

2.5. Fabrication of PANI-NSA+Ni memory devices

To fabricate the devices, initially the Indium doped Tin Oxide (ITO) coated onto polyethylene terephthalate (PET) substrates were cleaned with ethanol in an ultrasonicated bath for 5 minutes. Thereafter, PANI-NSA+Ni nanocomposites with a loading of (0.01 wt%) were mixed with PVP (used as binder) solution (1.0 wt%) to acquire a homogeneous mixture. Then, the 150 μm-thick nanocomposite film were drop-casted onto the ITO substrate by drop casting process. Subsequently, the top Ag electrode, with of 100 μm thickness, was deposited onto the PANI-NSA+Ni layer by using a conductive Ag paste. Average diameter of the Ag electrodes was about 3 mm. Finally, the devices were allowed to dry at room temperature for 48 hours prior to device property measurements. ITO/PANI-NSA/Ag device was also fabricated using similar method for comparison. The photograph of the as fabricated ITO/PANI-NSA+Ni/Ag device is shown in Fig. 1.

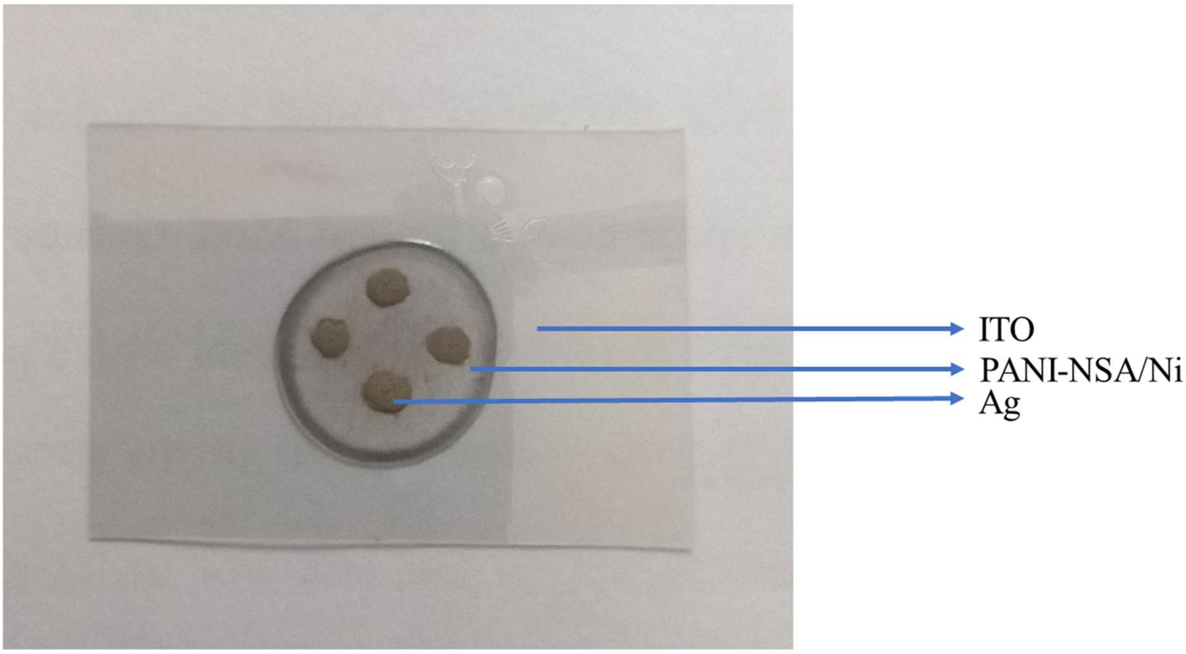

Fig. 1. The photograph of the fabricated device.

3. Results and discussion

3.1. Characterization

Tubular morphology of the as prepared polymer (PANI-NSA) and its nanocomposites PANI-NSA/Ni was visualized from the FE-SEM images as displayed in Figs 2(a) and (b), respectively. These images confirm the formation of nanotubes of PANI-NSA with smooth surface and the diameter varied between the range of 140-160 nm. On the other hand, because of supporting the Ni nanoparticles with spherical/nearly spherical shapes, the diameters of the PANI-NSA nanotubes are increased to about 200–220 nm range (Fig. 2b) having a rougher surface texture. Moreover, formation of Ni NPs onto the nanocomposite surface is verified with EDX (Figure 2c) and elemental mapping image (Fig. 2d) of C, O, S, and Ni for PANI-NSA+Ni NCs. The presence of pronounced Ni peak in the EDX spectrum and uneven distribution of Ni NPs onto the composite surface (Fig. 2d) established the effective deposition of Ni NPs onto the nanotubular PANI-NSA matrix.

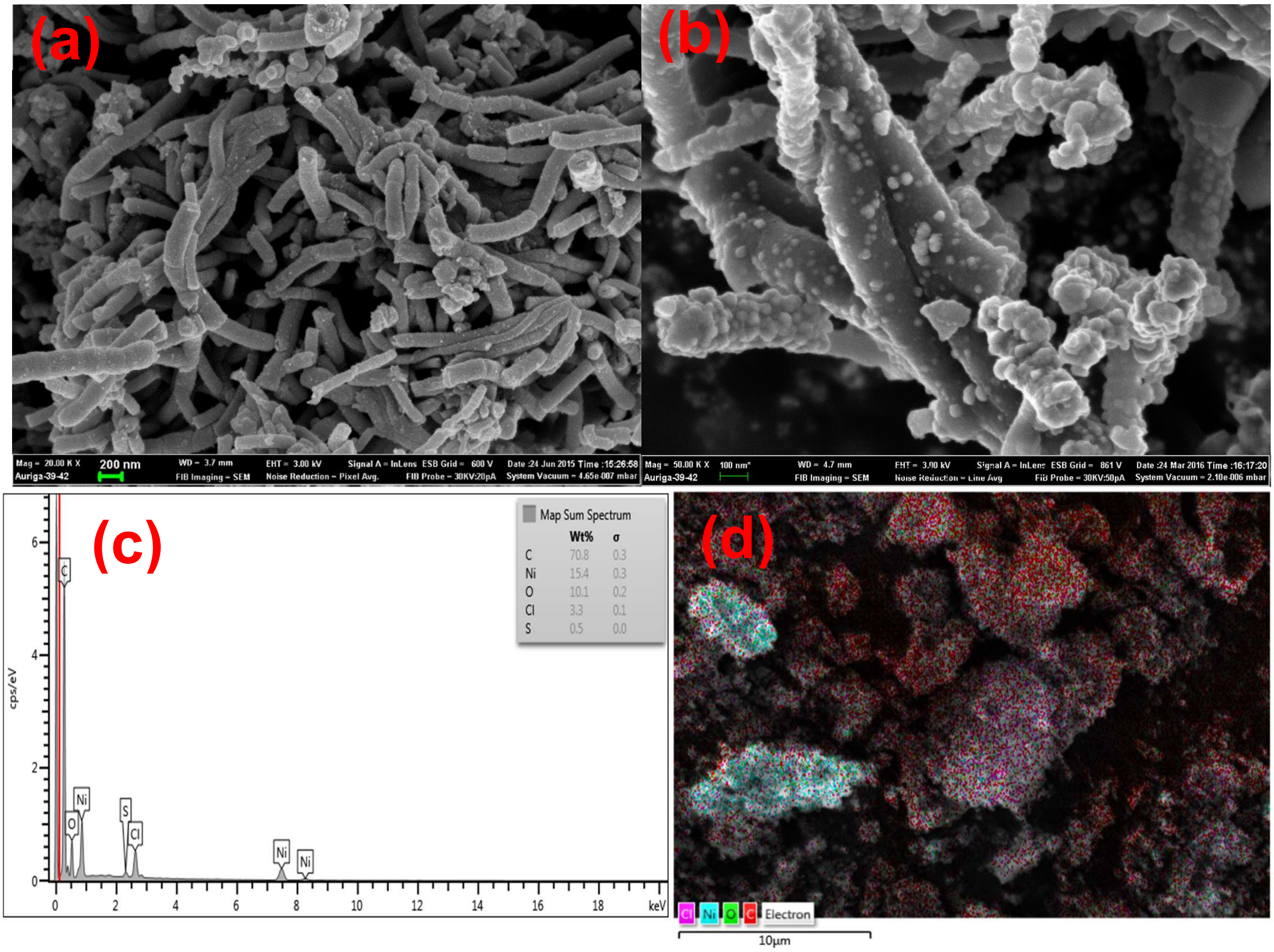

Fig. 2. SEM images of (a) PANI-NSA nanotubes, (b) PANI-NSA+Ni nanocomposites, (c) EDX spectrum and (d) Elemental mapping of PANI-NSA+Ni nanocomposites.

From the HR-TEM images of the polymer PANI-NSA and its PANI-NSA+Ni NCs as displayed in Figs. 3(a), (b) (c) and (d), it can be perceived that Ni nanoparticles are unevenly coated onto the PANI-NSA nanotubes smooth surfaced (Fig. 3a) matrix. The HR-TEM image of PANI-NSA+Ni (Fig 3d) showed clear crystal lattice fringes with inter planer spacing 0.208 nm which is in conformity with the face centred cubic (fcc) metallic Ni (111) crystal planes, demonstrating high crystallinity of the as formed Ni NPs.

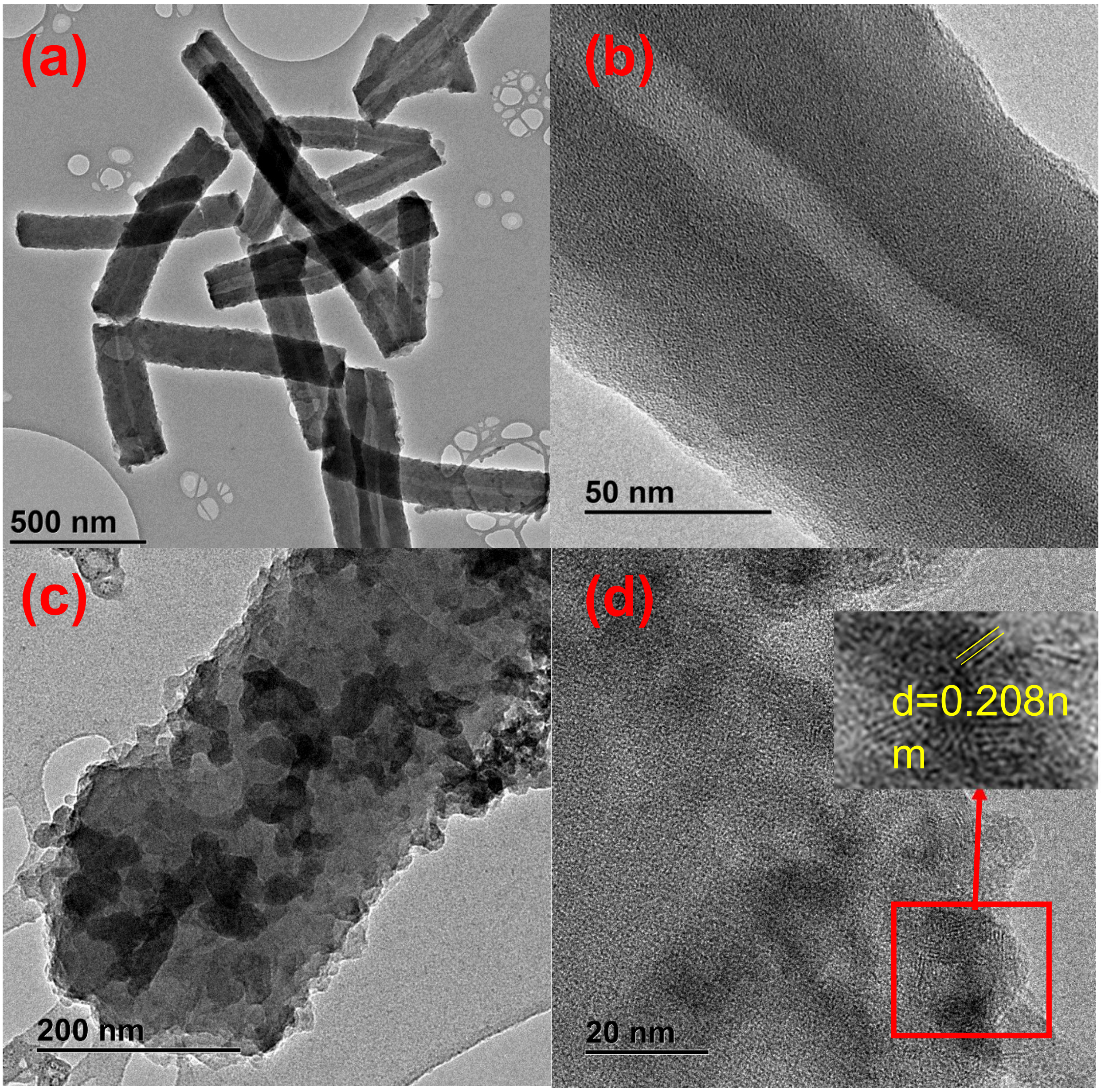

Fig. 3. HR-TEM image of (a) PANI-NSA nanotubes, (b) and (c) PANI-NSA+Ni nanocomposites.

The ATR-FTIR spectrum of the prepared PANI-NSA nanotubes as depicted in Fig. 4(a) was utilized to determine the chemical bonding structure. The vibrational stretching characteristics of quinonoid (Q) along with benzenoid (B) rings of the PANI polymer are occurred at 1591 cm^{-1} and 1494 cm^{-1} of the ATR-FTIR spectrum in Fig. 4 (a). The detected bands at 1283 cm^{-1} and 1223 cm^{-1} could be allocated to the stretching vibration of the C-N bonds inside Q-B-Q and B unites. Meanwhile, the frequency peaks at 1163 cm^{-1} and 811 cm^{-1} are the representative of stretching vibration of B-NH^{+}=Q and bending vibration of C-H aromatic rings within the backbone of PANI polymer [43]. The doping of sulfonic acid ($-SO_3H$) groups from 2-NSA within the polymer structure during polymerization was confirmed by the appearance of 1037 cm^{-1} and 693 cm^{-1} wave number bands in the FTIR-spectrum of PANI-NSA polymer [44]. Additionally, as observed in Fig. 4b it can be inferred that after formation of PANI-NSA+Ni composite nanotubes all the characteristic FTIR vibrational bands of PANI-NSA were red shifted to higher wave number.

The X-ray diffraction (XRD) pattern of bare PANI-NSA nanotubes and PANI-NSA+Ni composite nanostructures are depicted in Fig. 4(b). The strong intensity peaks detected at 2θ values of 9.1°, 21.7° and 25.7° are in conformity with the reflection from (001) (020) and (200) crystal planes with pseudo-orthorhombic cells of PANI-NSA polymer [40]. The sharp intensity peaks (Fig. 4a) of diffraction appeared at 2θ values of 44.7°, 52.1° and a small peak at 76.7°are resembled with the diffraction from (111), (200) and (220) crystal planes of zero valent or metallic Ni NPs (JCPDS cards No. 65-0380). These facts suggest that the Ni NPss are evidently grown onto the PANI-NSA nanotubes surface. Furthermore, at $2\theta = 20.01°$ and 25.1° the observed broad diffraction peaks (Fig. 4a) of the PANI-NSA nanotubes corroborating with the amorphous feature of the PANI polymer upon formation of nanocomposite [45]. These results specify a possible chemical interaction between the Ni NPs deposits and PANI-NSA nanotubes of the NCs.

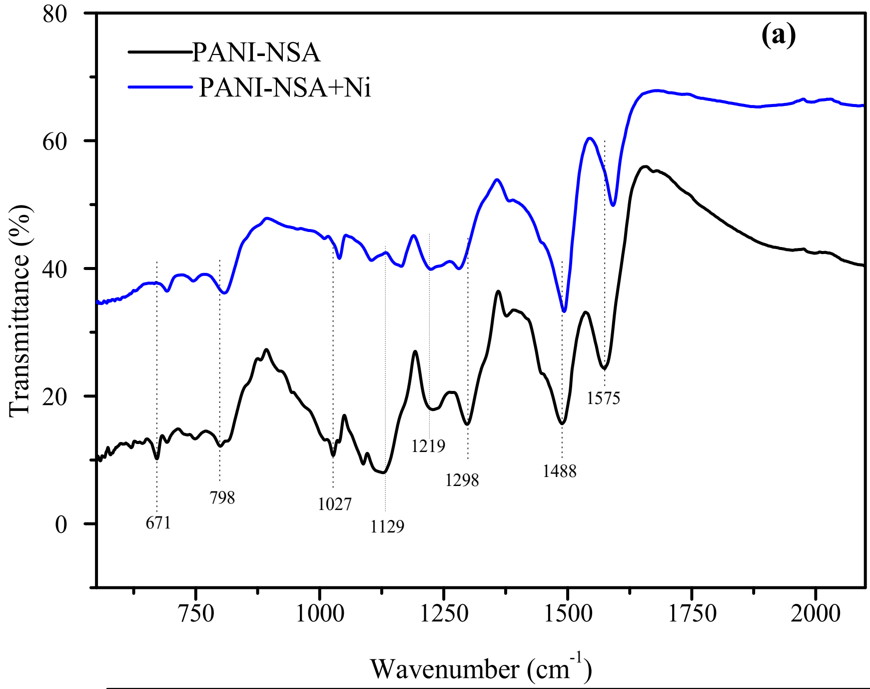

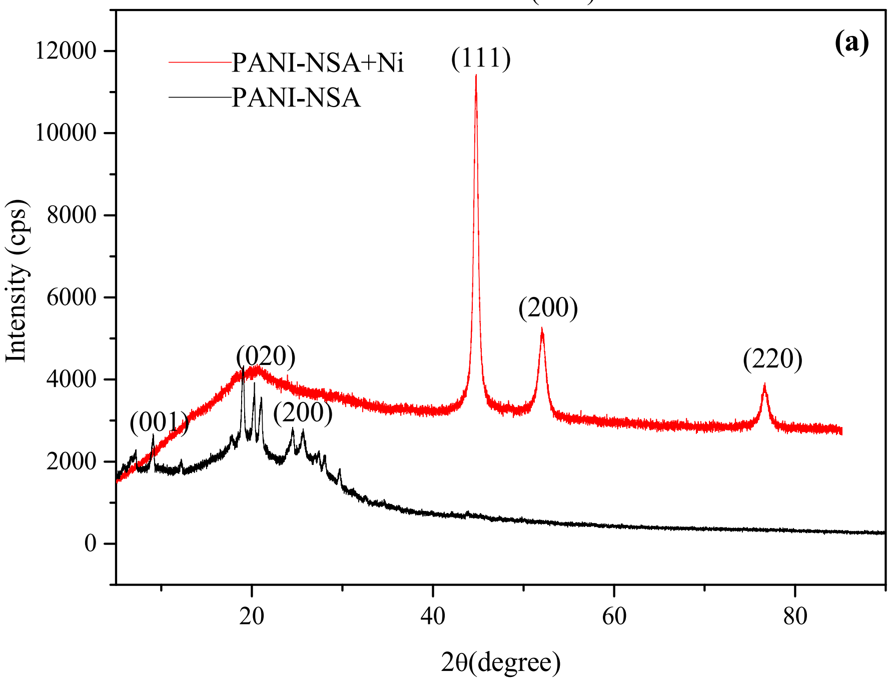

Fig. 4. (a) ATR-FTIR spectra of PANI-NSA nanotubes and PANI-NSA+Ni nanocomposites and (b) XRD patterns of PANI-NSA nanotubes and PANI-NSA+Ni nanocomposites.

Figure 5(a) represents the survey spectrum of the PANI-NSA+Ni nanocomposites undergone through XPS measurements. In the survey spectrum peaks of C 1s, N 1s, S 1s are the representative the binding energies of the PANI polymer doped with 2-NSA, while the originated Ni 2p binding energy peak is designated to the as grown Ni nanoparticles. These binding energy peaks endorsed the presence of both Ni and 2-NSA doped PANI components into the composite nanostructures. Figure 5(b) shows deconvoluted core level spectrum of N 1s. The peaks centred at 398.9 eV can be attributed to doped imine ($-NH^{+}=$) while binding energy peaks centred at 399.8 eV and 400.8 eV corroborated with benzenoid amine (-NH-), and cationic nitrogen atoms ($-NH^{\bullet+}$) representing polaron or bi-polaron, respectively [46]. Thus, approves effective doping of 2-NSA within PANI structure. Core level spectrum of Ni 2p as shown in Fig. 5(c) constitutes with doublets of Ni $2p_{1/2}$ and Ni $2p_{3/2}$ originating from transitions of multiple electrons. The main binding energy peak at about 855.8 eV along with its satellite (sat Ni $2p_{3/2}$) peak corresponds with peak of Ni $2p_{3/2}$ state, whereas the peak around 873.5 eV and its satellite peak corroborating with the Ni $2p_{1/2}$ state. These results confirm the occurrence of Ni^{2+} species onto the surface of PANI-NSA+Ni NCs [47]. Additionally, the presence of metallic Ni nanoparticles onto the nanocomposite surface was confirmed by the binding energy peak centred at 852.5 eV (2p3/2) of Ni 2p level [47]. Presence of less metallic Ni with less peak area compared to those of Ni^{2+} species (oxides or hydroxide of Ni) might be due to the fact that metallic Ni nanoparticles are highly susceptible to air oxidation which leads to the formation of a thin layer of Ni^{2+} species onto the surface of PANI-NSA+Ni NCs.

The room temperature (300 K) hysteresis curve i.e., magnetization (M) vs field (H) loop used to determine the magnetic property of the PANI-NSA+Ni NCs acquired in the range of -10000 Oe to +10000 Oe and is depicted in Fig. 5 (d). It is worth noticing from the M-H curve that PANI-NSA+Ni nanocomposites display the saturation magnetization (Ms) value of 16.6 emu/g which is the characteristic of a weak ferromagnetic material. The obtained Ms value of PANI-NSA+Ni nanocomposites is noticeably lesser than the Ms value of 55 emu/g Ni for bulk Ni at 300 K [48]. Existence of diamagnetic PANI-NSA polymer within the PANI-NSA+Ni NCs might be responsible for the suppression the M_S value to certain amount.

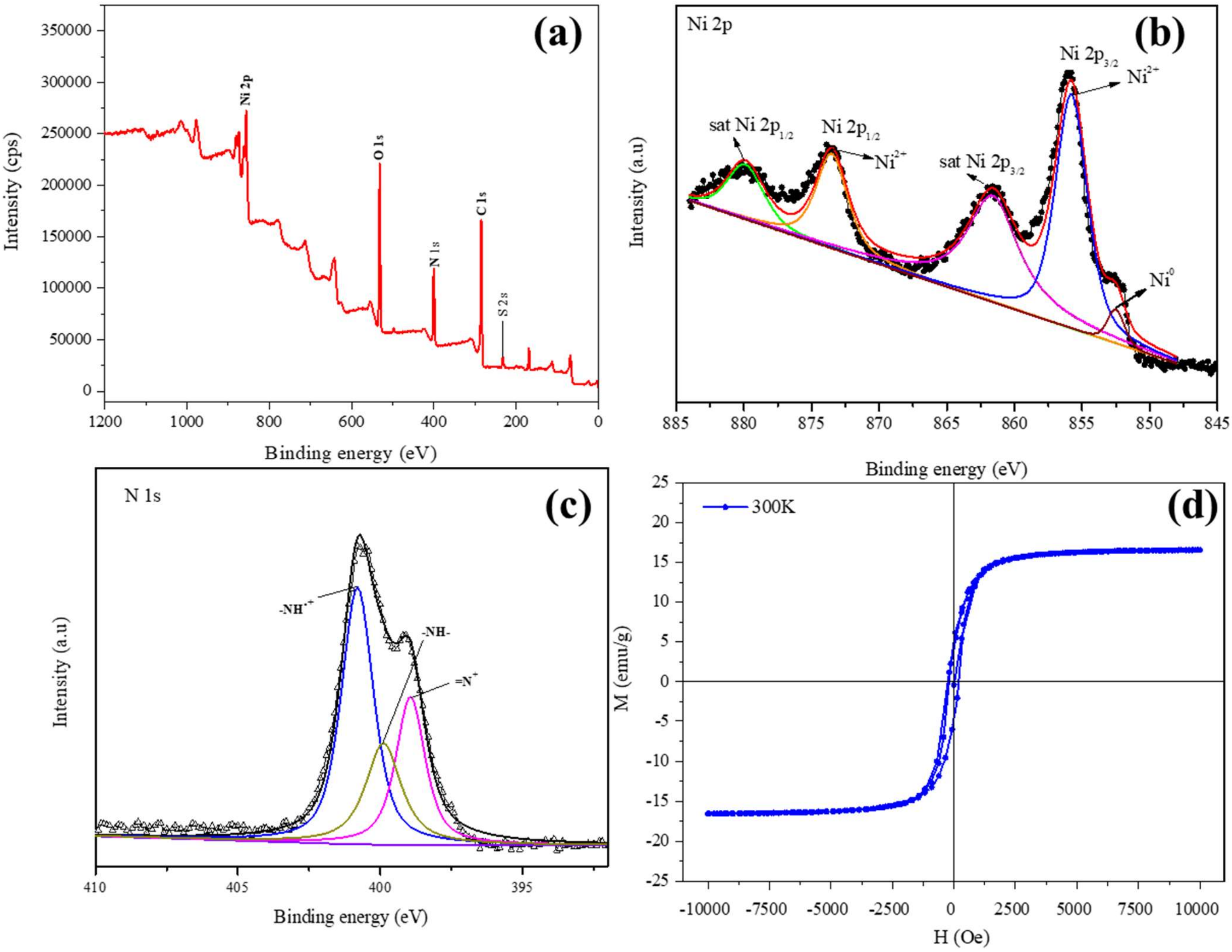

Fig. 5. (a) XPS survey spectrum of PANI-NSA+Ni, (b) N 1s core level spectrum of PANI-NSA+Ni, (c) Ni 2p spectrum of PANI-NSA+Ni and (d) M-H curve of PANI-NSA+Ni at 300K.

3.2. Current–voltage characteristics

Current-Voltage (I-V) characteristics of all the manufactured devices were obtained at ambient temperature subjected to the bias voltage applied to the top Ag electrode whereas the bottom ITO electrode was grounded. A compliance current was set to the value of 100 μA to prevent the permanent damage of all the devices. Figures 6 (a) and 6(b) display I-V curve of

ITO/PANI-NSA/Ag and ITO/PANI-NSA+Ni/Ag devices in linear scale where voltage bias was increased from 0 to +2V with 10 mV steps. From Fig. 6 it can be observed that an abrupt increase in current is occurred when the applied bias voltage is positive, which is called first Set process or the forming process. Because of the formation of conducting path the devices resistance is switched from the initial high resistance state (HRS) to a low resistance state (LRS). For the device with PANI-NSA as active layer the current remains almost zero up to the voltage 1.5V, called forming voltage, whereas for PANI-NSA+Ni device the forming process occur at a voltage of 1.72V. For the pure PVP film no switching behaviour was observed when tested under the same experimental conditions. Figs. 6 (c) and 6 (d) show I-V characteristics of ITO/PANI-NSA/Ag device and ITO/PANI-NSA+Ni/Ag device in semi-log scale for the first sweeping bias voltage of 0→+2→0→-2→0V, respectively. The direction of the resistive switching for the devices are shown by the arrows. After the set process, an applied voltage of -1.76V for PANI-NSA device and -1.47V for PANI-NSA+Ni device leads the resistance of the devices back to HRS and this process is called Reset, suggesting rapture of formed conducting path [49]. The dynamic of Reset for PANI-NSA is different than that of PANI-NSA+Ni. This might be because of different charge transport mechanisms involved for the two devices in the Reset process. Owing to the fact that the Set as well as Reset appear at opposite polarities, both PANI-NSA and PANI-NSA+Ni devices are categorized as bipolar resistive switching type device [50]. It is worth noticing from Fig. 6 that the PANI-NSA+Ni NCs device represents similar switching behaviour as that of PANI-NSA counterparts under the same operating conditions. However, the Set voltage for PANI-NSA is less than that of PANI-NSA+Ni device. Additionally, both the devices exhibit similar Set and Reset process even for multiple cycles (Fig. S1) with the ratio of on current and off current (Ion/Ioff) ~10^3, adequate towards the reading of an error-free digital data amongst logical 1 and logical 0 state [51-54]. Meanwhile, the acquired I-V curves for both the devices are asymmetric in nature, this might be related to the formation of stochastic and breakage of the conducting path [55]. Since for Ag/PANI-NSA/ITO device on 20th cycle resistive switching hysteresis loops were collapsed further studied were conducted on ITO/PANI-NSA+Ni/Ag devices only.

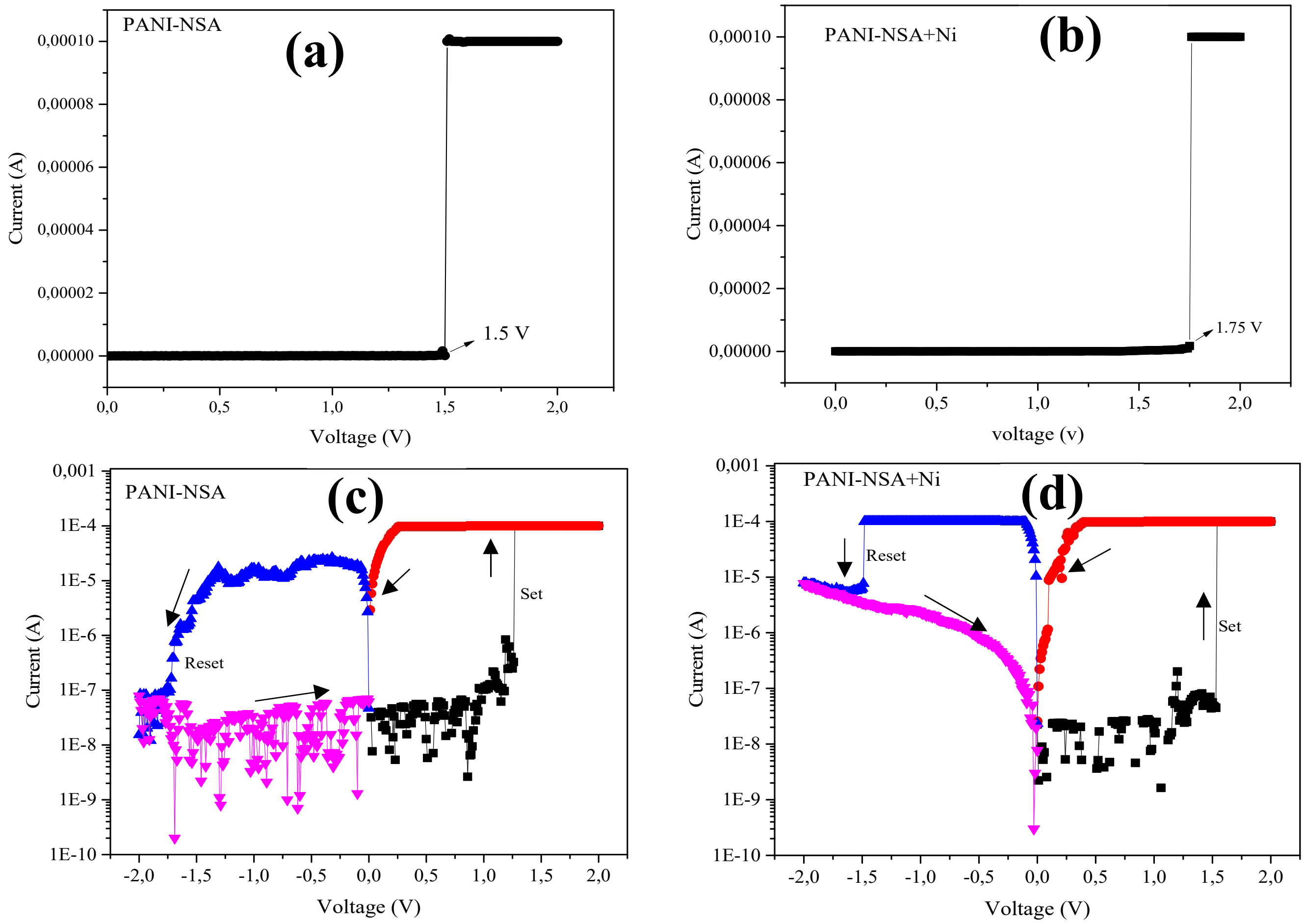

Fig. 6. I-V Characteristics of PANI-NSA and PANI-NSA+Ni device (a) and (b) forming curves in linear scales and (c) and (d) first sweep cycles in a semilogarithmic scale.

An endurance test was performed in order to explore the non-volatile memory characteristic of the ITO/PANI-NSA+Ni/Ag device. The endurance of the ITO/PANI-NSA+Ni/Ag device is investigated at a reading voltage of +0.5V which was in the form of a pulse signal for 200 cycles as depicted in Fig.7 a. It is perceived that over the cyclic tests the Ag/PANI-NSA+Ni/ITO device stays stable, with minor degradation or fluctuation in both ON and OFF state current. The average memory window which is defined as the HRS (5.72×10^6 Ω) and LRS (3.74×10^3 Ω) resistance ratio (HRS/LRS) is calculated as $\sim 1.5 \times 10^3$ and is almost constant for the whole endurance experiments. The acquired endurance test results suggest that PANI-NSA+Ni nanocomposites is a superior material for the application in non-volatile memory devices [56-58].

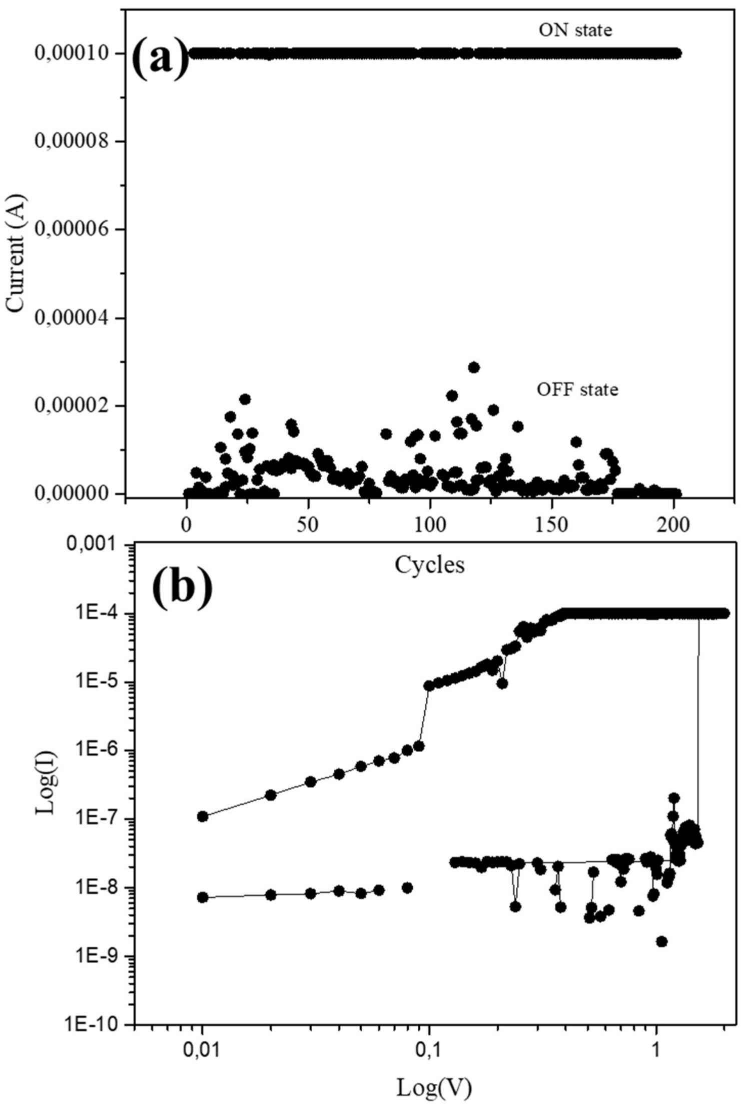

Fig. 7. (a) Endurance cycles and (b) Positive bias I-V characteristic in log-log scale.

3.3. Conduction and switching mechanism

Various theoretical models like interface-limited Scottky emission, interface limited Fowler-Nordheim, space charge limited conduction (SCLC), Ohmic conduction, tunnelling bulk limited Poole-Frenkel (PF) emission have been employed to explore the charge conduction and resistive switching mechanism of various materials. Herein, to explore the conduction mechanism of the PANI-NSA+Ni NCs device, experimentally acquired I-V data is presented on a log-log scale as shown in Fig 7(b) for the positive bias voltage. For different voltage regions different charge transport models can be fitted for the investigation of the resistive switching mechanism. It is worth noticing that up to the 0.8V voltage region in the HRS curve Ohmic charge transport model is in conformity with the experimental data (Fig. 8a) as the correlation coefficient (R^2) is ~ 0.98 for the HRS region. For the high voltage region of HRS current conduction followed by space charge limited Mott–Gurney law, where I (current) is proportional to V^2 (voltage^2) as represented by the Figs. 8 (b) and 8 (c) with higher R^2 values [59]. Beyond the bias voltage of 1.5V an abrupt increase in current is observed which lead to the device to the LRS. On reversing the voltage bias from 2-0V, the charge transport mechanisms are in good agreement with Mott- Grney law as shown in Fig 8 (d). The incidence of Ohmic conduction in the course of HRS owing to electrons generated thermally from the top Ag electrode, Ni nanoparticles of the nanocomposites as well as from the deprotonation process of the polyaniline. Meanwhile, during the LRS current conduction originated due to the trap controlled current conduction mechanism [49]. The detailed resistive switching mechanism of the PANI-NSA+Ni NCs is projected in the scheme 1. Initially, the resistance of the device originated from oxide layers of PANI-NSA+Ni sample. The existence of thin layer of oxides is due to the fact that Ni nanoparticles are highly susceptible to oxidation in the presence of air. The application of a positive voltage bias to the top Ag electrode, the generated oxygen ions resided on the surface drift towards the Ag electrode and constitute local intrinsic conductive filaments under the influence of electric force, causing Ohmic conduction at the lower portion of HRS of the device. The π electrons from PANI-NSA are also contributing towards the resistive switching process in the PANI-NSA+Ni nanocomposite device. Consequently, this switching process involves an electroforming process with a large positive bias voltage on resemblance with the oxygen ion migration switching [60-62]. On increasing the positive bias voltage, the number of oxygen ions (O^{2-}) increases which generate a conductive path amongst top and bottom electrodes and thereby the PANI-NSA+Ni device switches to LRS. Moreover, at the set process, protons are liberated from N-H sites of polyaniline and empty traps are occupied by produced electrons, leading to the resistance reduction of the layer, and therefore highest current is detected in the device. Reversal of the applied bias polarity, the migrating ions/electrons orient themselves in the opposite direction. In the Reset process as protonation of the PANI-NSA is dominant, the concentration of generated oxygen ions or free electrons is declined. The minimum number of electrons, empty traps, and filament breakage due to Joule's heating reduces the LRS and high resistance state was perceived in the nanocomposite device. Furthermore, oxidized (NiO) or metallic Ni which can be the either semi-conductive or conductive, dispersed onto the PANI-NSA matrix induce electric field lines which converge in the vicinity of nanoparticle's sites, and the electric field intensity around nanoparticles can significantly enhanced than those of the further section [49]. As the Ni nanoparticles improved the electric field, the O^{2-} ions surrounding the nanoparticles sites can easily move towards the top Ag electrode and leads to the formation of conducting path along the possible shortest route involving Ni nanoparticles compare to the other regions, that allows their generation possibility along the identical pathway in the repetitive resistive switching cycles [49].

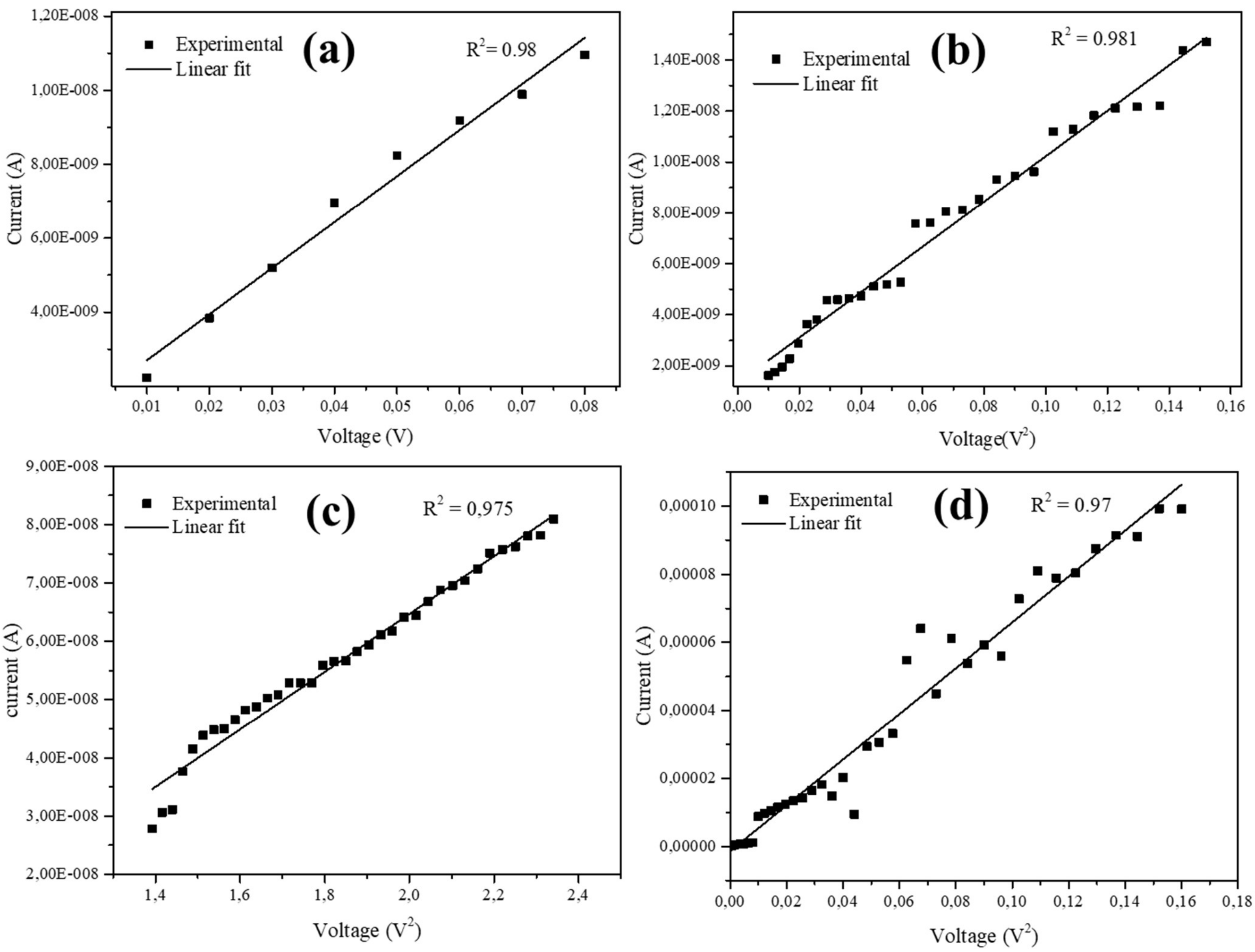

Fig. 8. (a) Low voltage HRS regime, (b) and (c) high voltage HRS region and (d) Low voltage LRS region.

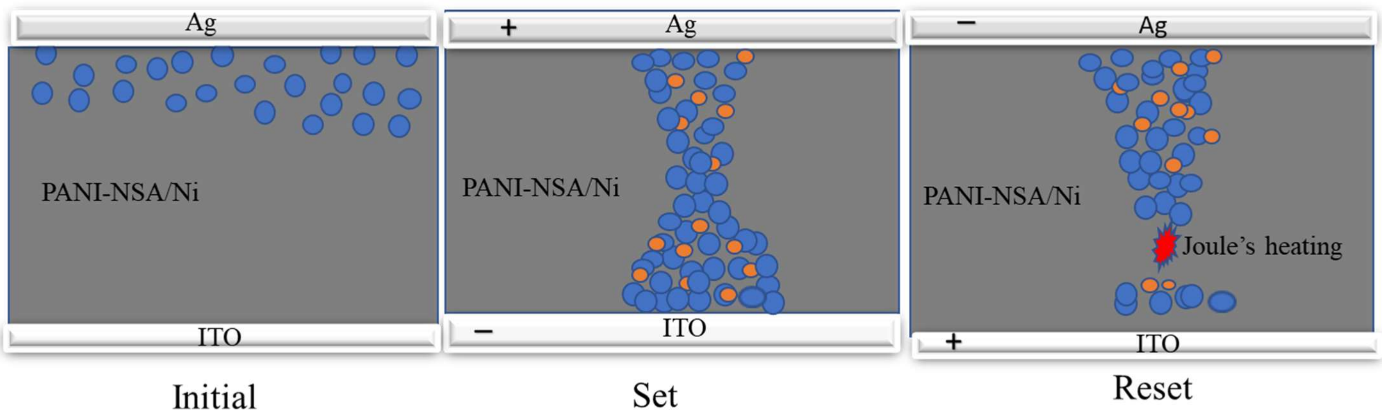

Scheme 1: Plausible resistive switching mechanism of PANI-NSA/Ni nanocomposites-

- Oxygen ions, -Free electron

4. Conclusion

In this work we have successfully synthesized tubular composite nanostructure of PANI-NSA nanotubes and magnetic Ni nanoparticles. FE-SEM and HR-TEM images confirm nanotubular morphology of the prepared nanocomposites. Structural characterization suggests inclusion of metallic weak ferromagnetic Ni nanoparticles onto PANI-NSA matrix. The I-V characteristic of the ITO/PANI-NSA+Ni/Ag device and the device structure with PANI-NSA as active layer displayed bipolar resistive switching behaviour with an I_{ON}/I_{OFF} ~10^3. An average memory widow of ~$1.5X10^3$ was detected over 200 stable switching cycle. The experimental I-V data are in good conformity with the Ohmic conduction model for lower voltage region of HRS state, where as space charge limited conduction mechanism was observed for higher voltage region for HRS state. Space charge limited conduction model was also in well conformity with experimental data for LRS regime. Possible conducting path formation with oxygen ions, free electrons, and deprotonation of PANI polymer were identified as the major origin of resistive switching process. These results infers that the PANI-NSA+Ni NCs can be considered as an alternative potential nanostructures material for non-volatile resistive switching memory device application.

Acknowledgement

MB is appreciative to the National Research Foundation (NRF), South Africa, for providing a post-doctoral fellowship under the grant number UID: 132732. The authors like to acknowledge the chemical engineering department, University of Pretoria, South Africa, for providing infrastructure for the research activity.

References

[1] Jeong D S, Thomas R and Katiyar R S 2012 *Rep. Prog. Phys.* **75** 076502
[2] Pan F, Gao S, Chen C, Song C and Zeng F 2014 *Mat. Sci. Eng*. R 831-59
[3] Yang J J, Strukov D B and Stewart D R 2013 *Nat. Nanotechnol*. **8** 13-24
[4] Zhao M, Gao B, Tang J, Qian H and Wu H, 2020 *Appl. Phys. Rev.* **7** 011301
[5] Jain S, Ankit A, Chakraborty I, Gokmen T, Rasch M, Haensch Roy W K and Raghunathan A 2019 *IBM J. Res. Dev.* **63** 10:1-10:13
[6] Xiang D, Liu T, Xu J, Tan J Y, Hu Z, Lei B, Zheng Y, Wu J, Neto A H C, Liu L and Chen W 2018 *Nat. Commun*. **9** 2966
[7] Tan H, Liu G, Zhu X, Yang H, Chen B, Chen X, Shang J, Lu W D, Wu Y and Li R W 2015 *Adv. Mater.* **27** 2797-803
[8] Siemon A*, et al.* 2015 *Adv. Funct. Mater.* **25** 6414-23
[9] Liu S, Lu N, Zhao X, Xu H, Banerjee W, Lv H, Long S, Li Q, Liu Q and Liu M 2016 *Adv. Mater.* **28** 10623-29
[10] Zhang B, Fan F, Xue W *et al*. 2019 *Nat. Commun.* **10** 736
[11] Li H, Xu Q, Li N, Sun R, Ge J, Lu J, Gu H and Yan FA 2010 *J. Am. Chem. Soc*. **132** 5542-43
[12] Zhao K, Yu F, Liu W, Huang Y, Said A A, Li Y and Zhang Q 2020 *J. Org. Chem.* **85** 101-7
[13] Asadi K, de Leeuw D M, de Boer B and Blom P W M 2008 *Nat Mater.* **7** 547-50.
[14] Leydecker T, Herder M, Pavlica E, Bratina G, Hecht S, Orgiu, E and Samorì P 2016 *Nat. Nanotechnol.* **11** 769-75
[15] Gu P, Gao J, Lu C *et al*. 2014 *Mater. Horiz.***1** 446-51
[16] Xiao J, Yin Z, Li H, Zhang Q, Boey F, Zhang H and Zhang Q 2010 *J. Am. Chem. Soc.* **132** 6926-28
[17] Hwang B and Lee J S 2019 *Adv. Electron. Mater.* **5** 1800519
[18] Yi X, Yu Z, Niu X, Shang J, Mao G, Yin T, Yang H, Xue W, Dhanapal P, Qu S, Liu G, and Li R W 2019 *Adv. Electron Mater.* **5** 1800655
[19] Yao Z, Pan L, Liu L, Zhang J, Lin Q, Ye Y, Zhang Z, Xiang S and Chen B 2019 *Sci. Adv.* **5** 4515
[20] Solanki A, Guerrero A, Zhang Q, Bisquert J and Sum T C 2019 *J. Phys. Chem. Lett*. **1** 463-70
[21] Bertolazzi S, Bondavalli P, Roche S, San T, Choi S Y, Colombo L, Bonaccorso F and Samorì P, 2019 *Adv. Mater*. **31** 1806663
[22] Wang H, Meng F, Zhu B, Leow W R, Liu Y and Chen X 2015 *Adv. Mater.* **27** 7670-7676.
[23] Li Y, Chen L, Ai Y, Hong E Y, Chan A K and Yam V W W 2017 *J. Am. Chem. Soc.* **139** 13858-66
[24] Bhadra J, Alkareem A and Al-Thani N 2020 *J. Polym. Res.* **27** 122
[25] Tanguy N R, Thompson M and Yan N 2018 *Sens. Actuators*. B **257** 1044–64
[26] Sen T, Mishra S and Shimpi N G *RSC Advs.* **6** 42196–222
[27] Balint R, Cassidy N J and Cartmell S H 2014 *Acta Biomater.* **10** 2341–53
[28] Guo S, Dong S and Wang E 2009 *Small* **5** 1869–76
[29] Huang C C, Wen T C and Wei Y 2010 *Mater. Chem. Phys.* **122** 392–96
[30] Jia W, Su L and Lei Y 2011 *Biosens. Bioelectron.* **30** 158–64
[31] Eftekhari A, Lei L and Yang Y 2017 86-107
[32] Bhaumik M, Maity A and Brink H G 2021 *Chem. Eng. J.* **417** 127910
[33] Wu G, More K L, Johnston C M and Zelenay P 2011 *Science* **332** 443–47
[34] Tseng R J, Huang J, Ouyang J, Kaner R B and Yang Y 2004 *Nano Lett.* **5** 1077-80

[35] Pincella F, Camorani P and Erokhin V 2011 *Appl. Phys. A* **104** 1039–46
[36] Erokhina S, Sorokin V and Erokhin V 2015 *Electron. Mater. Lett*. **5** 11801-805
[37] Chiolerio A, Bocchini S, Crepaldi M, Bejtka K and Pirri C F, 2017 *Synthetic Metals* **229** 72-81
[38] Lapkin D A, Emelyanov AV, Demin VA, et al. 2018 *Appl. Phys. Lett*. **112** 043302
[39] Lapkin D A, Korovin A N , Malakhov SN, et al. 2020 Adv Electron Mater 6 2000511
[40] Eskandari F, Shabani P and Yousefi R 2020 *Org. Electron*. **79** 105628
[41] Patil K T, Nirmal K A, Jadhav S A, Patil S R, Dongale T D, Kim D and Patil P S 2021 *Materialia* **15** 101026
[42] Higuchi R, Lilak S, Sillin H O, Tsuruoka T, Kunitake M, Nakayama T, Gimzewski J K and Stieg A Z 2023 *Sci Technol. Adv. Mater.* **24** 2178815.
[43] Zhang Z, Wei Z, Zhang L and Wan M 2005 *Acta Mater.* **53** 1373–79
[44] Huang J and M. Wan, 1999 *J. Polym. Sci. A: Polym. Chem.* **37** 151–57
[45] Bhaumik M, Gupta, V K and Maity A 2018 *J. Environ. Chem. Eng.* **6** 2514–27
[46] Wei X L, Fahlman M and Epstein A J1999 *Macromolecules* **32** 3114–17
[47] Wang J, Zhao Q, Hou H, Wu Y, Yu W, Ji X and Shao L 2017 *RSC Adv.* **7** 14152–58
[48] Bozorth R M 1951 D. Van Nostrand Company Inc, New York.
[49] Xu Z, Gao M, Yu L, Xu X and Jiang Y 2014 *ACS Appl. Mater. Interfaces* **6** 17823-30
[50] Lee J, Lee S and Noh T, 2015 *Appl. Phys. Rev.* **2** 031303
[51] Ji Y, Zeigler D F, Lee D S, Choi H, Jen A K Y, Ko H C and. Kim T W 2013 *Nat. Commun.* **4** 2707
[52] Rani A, Velusamy D B, Mota M, Jang F and Kim Y H 2017 *Adv. Funct. Mater.* **27** 160460
[53] Kim R H, Lee J, Kim K L, Cho S M, Kim D H and Park C 2017 *Small* **24** 1603971
[54] Ling H, Yi M, Nagai M, Xie L, Wang L, Hu B and Huang W 2017 *Adv. Mater.* **29** 1701333
[55] Khalid M 2019 *Trans. Electr. Electron. Mater.* **20** 289–98
[56] Hassan G, Ali S, Bae J and Lee C 2017 *Appl. Phys. A* **123** 256
[57] He Y, Ma G, Zhou X, Cai H, Liu C, Zhang J and Wang H 2019 *Org. Electron*. **68** 230–35
[58] Minnekhanov A, Emelyanov A, Lapkin D, Nikiruy K, Shvetsov B, Nesmelov A, Rylkov V, Demin V and Erokhin V 2019 *Sci. Rep*. **9** 10800
[59] Mott F N and Gurney R W 1940 *Electronic Processes in Ionic Crystals, 1st ed*. Oxford University Press
[60] Long S B, Cagli C, Ielmini D, Liu M, and Sun˜e J 2011 *IEEE Electron Device Lett.* **32** 150−72
[61] Long S B, Cagli C, Ielmini D, Liu M and Sun˜e J 2012 *J. Appl. Phys.* **111** 074508
[62] Xu Z D, Yu L N, Xu X G, Miao J and Jiang Y 2014 *Appl. Phys. Lett.* **104** 192903